CLEO CONF95-21
EPS0182
June 30, 1995

MEASUREMENTS OF THE RATIOS $\mathcal{B}(D_s^+ \to \eta\ell^+\nu)/\mathcal{B}(D_s^+ \to \phi\ell^+\nu)$ AND $\mathcal{B}(D_s^+ \to \eta'\ell^+\nu)/\mathcal{B}(D_s^+ \to \phi\ell^+\nu)$.

J. Bartelt,[1] S.E. Csorna,[1] V. Jain,[1] S. Marka,[1] D. Gibaut,[2] K. Kinoshita,[2] P. Pomianowski,[2] B. Barish,[3] M. Chadha,[3] S. Chan,[3] D.F. Cowen,[3] G. Eigen,[3] J.S. Miller,[3] C. O'Grady,[3] J. Urheim,[3] A.J. Weinstein,[3] F. Würthwein,[3] D.M. Asner,[4] M. Athanas,[4] D.W. Bliss,[4] W.S. Brower,[4] G. Masek,[4] H.P. Paar,[4] J. Gronberg,[5] C.M. Korte,[5] R. Kutschke,[5] S. Menary,[5] R.J. Morrison,[5] S. Nakanishi,[5] H.N. Nelson,[5] T.K. Nelson,[5] C. Qiao,[5] J.D. Richman,[5] D. Roberts,[5] A. Ryd,[5] H. Tajima,[5] M.S. Witherell,[5] R. Balest,[6] K. Cho,[6] W.T. Ford,[6] M. Lohner,[6] H. Park,[6] P. Rankin,[6] J.G. Smith,[6] J.P. Alexander,[7] C. Bebek,[7] B.E. Berger,[7] K. Berkelman,[7] K. Bloom,[7] T.E. Browder,[7*] D.G. Cassel,[7] H.A. Cho,[7] D.M. Coffman,[7] D.S. Crowcroft,[7] M. Dickson,[7] P.S. Drell,[7] D.J. Dumas,[7] R. Ehrlich,[7] R. Elia,[7] P. Gaidarev,[7] M. Garcia-Sciveres,[7] B. Gittelman,[7] S.W. Gray,[7] D.L. Hartill,[7] B.K. Heltsley,[7] S. Henderson,[7] C.D. Jones,[7] S.L. Jones,[7] J. Kandaswamy,[7] N. Katayama,[7] P.C. Kim,[7] D.L. Kreinick,[7] T. Lee,[7] Y. Liu,[7] G.S. Ludwig,[7] J. Masui,[7] J. Mevissen,[7] N.B. Mistry,[7] C.R. Ng,[7] E. Nordberg,[7] J.R. Patterson,[7] D. Peterson,[7] D. Riley,[7] A. Soffer,[7] P. Avery,[8] A. Freyberger,[8] K. Lingel,[8] C. Prescott,[8] J. Rodriguez,[8] S. Yang,[8] J. Yelton,[8] G. Brandenburg,[9] D. Cinabro,[9] T. Liu,[9] M. Saulnier,[9] R. Wilson,[9] H. Yamamoto,[9] T. Bergfeld,[10] B.I. Eisenstein,[10] J. Ernst,[10] G.E. Gladding,[10] G.D. Gollin,[10] M. Palmer,[10] M. Selen,[10] J.J. Thaler,[10] K.W. Edwards,[11] K.W. McLean,[11] M. Ogg,[11] A. Bellerive,[12] D.I. Britton,[12] E.R.F. Hyatt,[12] R. Janicek,[12] D.B. MacFarlane,[12] P.M. Patel,[12] B. Spaan,[12] A.J. Sadoff,[13] R. Ammar,[14] P. Baringer,[14] A. Bean,[14] D. Besson,[14] D. Coppage,[14] N. Copty,[14] R. Davis,[14] N. Hancock,[14] S. Kotov,[14] I. Kravchenko,[14] N. Kwak,[14] Y. Kubota,[15] M. Lattery,[15] M. Momayezi,[15] J.K. Nelson,[15] S. Patton,[15] R. Poling,[15] V. Savinov,[15] S. Schrenk,[15] R. Wang,[15] M.S. Alam,[16] I.J. Kim,[16] Z. Ling,[16] A.H. Mahmood,[16] J.J. O'Neill,[16] H. Severini,[16] C.R. Sun,[16] F. Wappler,[16] G. Crawford,[17] R. Fulton,[17] D. Fujino,[17] K.K. Gan,[17] K. Honscheid,[17] H. Kagan,[17] R. Kass,[17] J. Lee,[17] M. Sung,[17] C. White,[17] A. Wolf,[17] M.M. Zoeller,[17] X. Fu,[18] B. Nemati,[18] W.R. Ross,[18] P. Skubic,[18] M. Wood,[18] M. Bishai,[19] J. Fast,[19] E. Gerndt,[19] J.W. Hinson,[19] T. Miao,[19] D.H. Miller,[19] M. Modesitt,[19] E.I. Shibata,[19] I.P.J. Shipsey,[19] P.N. Wang,[19] L. Gibbons,[20] S.D. Johnson,[20] Y. Kwon,[20] S. Roberts,[20] E.H. Thorndike,[20] T.E. Coan,[21] J. Dominick,[21] V. Fadeyev,[21] I. Korolkov,[21] M. Lambrecht,[21] S. Sanghera,[21] V. Shelkov,[21] T. Skwarnicki,[21] R. Stroynowski,[21] I. Volobouev,[21] G. Wei,[21] M. Artuso,[22] M. Gao,[22] M. Goldberg,[22] D. He,[22] N. Horwitz,[22] S. Kopp,[22] G.C. Moneti,[22] R. Mountain,[22] F. Muheim,[22] Y. Mukhin,[22] S. Playfer,[22] S. Stone,[22] and X. Xing[22]

(CLEO Collaboration)

[1] *Vanderbilt University, Nashville, Tennessee 37235*
[2] *Virginia Polytechnic Institute and State University, Blacksburg, Virginia, 24061*
[3] *California Institute of Technology, Pasadena, California 91125*
[4] *University of California, San Diego, La Jolla, California 92093*
[5] *University of California, Santa Barbara, California 93106*
[6] *University of Colorado, Boulder, Colorado 80309-0390*
[7] *Cornell University, Ithaca, New York 14853*
[8] *University of Florida, Gainesville, Florida 32611*
[9] *Harvard University, Cambridge, Massachusetts 02138*
[10] *University of Illinois, Champaign-Urbana, Illinois, 61801*
[11] *Carleton University, Ottawa, Ontario K1S 5B6 and the Institute of Particle Physics, Canada*
[12] *McGill University, Montréal, Québec H3A 2T8 and the Institute of Particle Physics, Canada*
[13] *Ithaca College, Ithaca, New York 14850*
[14] *University of Kansas, Lawrence, Kansas 66045*
[15] *University of Minnesota, Minneapolis, Minnesota 55455*
[16] *State University of New York at Albany, Albany, New York 12222*
[17] *Ohio State University, Columbus, Ohio, 43210*
[18] *University of Oklahoma, Norman, Oklahoma 73019*
[19] *Purdue University, West Lafayette, Indiana 47907*
[20] *University of Rochester, Rochester, New York 14627*
[21] *Southern Methodist University, Dallas, Texas 75275*
[22] *Syracuse University, Syracuse, New York 13244*

Abstract

Using the CLEO II detector at the Cornell Electron Storage Ring (CESR), we observe clean signals in both $D_s^+ \to \eta \ell^+ \nu$ and $D_s^+ \to \eta' \ell^+ \nu$ decay channels. We normalize the yields in these pseudoscalar channels to the yield in the vector channel $D_s^+ \to \phi \ell^+ \nu$, and measure $\mathcal{B}(D_s^+ \to \eta e^+ \nu)/\mathcal{B}(D_s^+ \to \phi e^+ \nu) = 1.24 \pm 0.12 \pm 0.15, \mathcal{B}(D_s^+ \to \eta' e^+ \nu)/\mathcal{B}(D_s^+ \to \phi e^+ \nu) = 0.43 \pm 0.11 \pm 0.07$. We compare the vector to pseudoscalar ratios in the D and D_s^+ semileptonic sectors, and measure $\mathcal{B}(D_s^+ \to \eta' e^+ \nu)/\mathcal{B}(D_s^+ \to \eta e^+ \nu) = 0.35 \pm 0.09 \pm 0.07$.

*Permanent address: University of Hawaii at Manoa

In B semileptonic decays, we measure $|V_{cb}|$ and $|V_{ub}|$ using the theoretical predictions on form factors. It is important to test and improve these theoretical predictions. In charm semileptonic decays, the absolute scale of form factors can be measured, since Cabibbo-Kobayashi-Masukawa (CKM) matrix elements, $|V_{cs}|$ and $|V_{cd}|$ are well known from unitarity. In particular, theoretical predictions for $b \to u\ell^-\overline{\nu}$ must be improved in order to determine $|V_{ub}|$ and studies of charm semileptonic decay will provide useful information.

One of the outstanding problems in charm semileptonic decay is the disagreement on the vector to pseudoscalar ratio, $\mathcal{B}(D \to \overline{K^*}e^+\nu)/\mathcal{B}(D \to \overline{K}e^+\nu)$ [1–3]. The experimental world average of this ratio is 0.56 ± 0.06, while theoretical predictions generally range from 0.8 to 1.2 [4–9]. However, Ball *et al.* predict 0.50 ± 0.15 with the QCD sum rules [10] and the recent ISGW2 model gives 0.54 for the ratio [11]. It is of interest to repeat these types of measurements in the D_s^+ sector, where the initial and final hadrons differ by the substitution of a light quark by a strange quark. While D^0 and D^+ semileptonic decays have been studied in detail, in the D_s^+ sector only the $D_s^+ \to \phi\ell^+\nu$ decay has been extensively studied. Fermilab experiment E653 has seen the evidence for $D_s^+ \to (\eta+\eta')\mu^+\nu$ [12]. In this paper we report the first measurements of $\mathcal{B}(D_s^+ \to \eta e^+\nu)$ and $\mathcal{B}(D_s^+ \to \eta' e^+\nu)$ normalized to $\mathcal{B}(D_s^+ \to \phi e^+\nu)$, and the vector to pseudoscalar ratio, *i.e.*, $\mathcal{B}(D_s^+ \to \phi e^+\nu)/\mathcal{B}(D_s^+ \to (\eta + \eta')e^+\nu)$, for D_s^+ semileptonic decays. The data include both muons and electrons. Phase space corrections have been applied to the muon data to present electron branching ratios [13].

The data consists of an integrated luminosity of 3.11 fb^{-1} of e^+e^- collisions recorded with the CLEO II detector at the Cornell Electron Storage Ring (CESR). The data sample contains about 3.7 million $e^+e^- \to c\bar{c}$ events taken at center-of-mass energies on the $\Upsilon(4S)$ resonance and in the nearby continuum ($\sqrt{s} \sim 10.6$ GeV). The CLEO II detector is a solenoidal detector with 67 tracking layers and a CsI electromagnetic calorimeter that provides excellent π^0 and η reconstruction [14].

The major semileptonic decay modes of D_s^+ meson are the ones with ϕ, η or η' meson in the final state. Due to the undetected neutrino, we cannot fully reconstruct $D_s^+ \to X\ell^+\nu$ ($X \equiv \phi, \eta$ or η') decays. However, there are few processes which produce both a ϕ, η or η' meson and a lepton contained in the same jet. Consequently, this correlation can be used to extract a clean $D_s^+ \to X\ell^+\nu$ signal. The backgrounds due to misidentified leptons and to random X–lepton combinations can be reliably estimated, and the possible contaminations from other decay modes are shown to be small. We can reduce these backgrounds further for $D_s^+ \to \eta\ell^+\nu$, which has sufficient statistics, by identifying the low energy photon from the $D_s^{*+} \to D_s^+\gamma$ decay. We refer to this second method as the D_s^{*+} tag analysis. We measure $\mathcal{B}(D_s^+ \to \eta e^+\nu)/\mathcal{B}(D_s^+ \to \phi e^+\nu)$ and $\mathcal{B}(D_s^+ \to \eta' e^+\nu)/\mathcal{B}(D_s^+ \to \phi e^+\nu)$ by extracting the yields of $D_s^+ \to \phi\ell^+\nu$, $D_s^+ \to \eta\ell^+\nu$ and $D_s^+ \to \eta'\ell^+\nu$ events with the non D_s^{*+} tag analysis. We apply the D_s^{*+} tag analysis to extract the yields of $D_s^+ \to \eta\ell^+\nu$ and $D_s^+ \to \phi\ell^+\nu$ events and measure $\mathcal{B}(D_s^+ \to \eta e^+\nu)/\mathcal{B}(D_s^+ \to \phi e^+\nu)$. The two values of $\mathcal{B}(D_s^+ \to \eta e^+\nu)/\mathcal{B}(D_s^+ \to \phi e^+\nu)$ are averaged.

Lepton candidates are restricted to the kinematic regions in which the lepton identification efficiencies and hadron misidentification rates are well understood. Hence, electron and muon candidates are restricted to lie in the fiducial regions $|\cos\theta| < 0.71$ and $|\cos\theta| < 0.81$, respectively, where θ is the polar angle of the track with respect to the beam axis. Electron candidates must have momenta above 1.0 GeV/c for the non D_s^{*+} tag analysis, but above 0.7 GeV/c for the D_s^{*+} tag analysis to get more statistics. Electrons are identified by comparing their ionization energy loss, time-of-flight, and energy deposited in the electromagnetic calorimeter with that expected for true electrons. Electrons from photon conversions and Dalitz decays of π^0's are rejected by pairing electron candidates with all other oppositely charged tracks in the event and rejecting those which have both small separation and parallel trajectories at their point of closest approach. Muon candidates in the region $|\cos\theta| < 0.61$ are required to have momenta above 1.5 GeV/c and those in the region $|\cos\theta| > 0.61$ are required to have momenta above 1.9 GeV/c. Muons are identified by matching charged tracks to hits in the muon detectors. In order to be identified as a muon, a track must penetrate at least 5 interaction lengths of iron.

We identify ϕ candidates by using the decay mode $\phi \rightarrow K^+K^-$. The ϕ candidates are required to have momenta greater than 1.0 GeV/c. Charged kaon candidates must have ionization energy loss and time-of-flight consistent with that expected for true kaons. Because of the small q^2 value associated with the decay $\phi \rightarrow K^+K^-$, the kaons tend to overlap in the drift-chamber. This makes it difficult to accurately simulate the ionization energy loss. In order to avoid this problem, the momentum dependent efficiencies for identifying ϕ mesons are obtained from the data by comparing the inclusive yield of all ϕ's before and after particle identification. These efficiencies are then combined with the predicted ϕ momentum spectrum from $D_s^+ \rightarrow \phi\ell^+\nu$ Monte Carlo events to give the total ϕ identification efficiency.

We use the decay mode $\eta \rightarrow \gamma\gamma$ to select η candidates. The photon candidates are restricted to lie in the fiducial region, $|\cos\theta| < 0.81$. We require that the lateral shower shape of photons be consistent with that expected for true photons. We require that $|\cos\theta_{decay}| < 0.9$, where θ_{decay} is the photon decay angle in the η rest frame with respect to the η direction in the laboratory. Backgrounds due to low momentum photons tend to peak at $|\cos\theta_{decay}| = 1$. Since most photons are daughters of π^0 decays, we eliminate any photon which, when combined with another photon, makes a mass combination consistent with the π^0 mass ($\pm 2.5\sigma$) and has a π^0 momentum greater than 0.8 GeV/c. The momenta of η candidates are required to be greater than 1.0 GeV/c.

We identify η' candidates via the decay chain $\eta' \rightarrow \eta\pi^+\pi^-$, $\eta \rightarrow \gamma\gamma$ with the selection of η candidates as explained above except that we require the momentum of the η to be greater than 0.6 GeV/c. We also require the invariant mass of the two photons from $\eta \rightarrow \gamma\gamma$ decays to be consistent with the η mass ($\pm 2.0\sigma$) to reduce the random combinations of two photons. We require the momenta of η' candidates to be greater than 1.0 GeV/c. Charged pion candidates must have ionization energy loss and time-of-flight consistent with that expected for true pions. The pion identification efficiency is obtained from inclusive η' data in the same manner as the kaon identification efficiency for ϕ reconstruction.

To suppress the combinatoric background from $\Upsilon(4S)$ events which tend to be more spherical, we require that the ratio of Fox-Wolfram moments [15], $R_2 = H_2/H_0$, be greater than 0.30 for each event. We require that the momentum of X candidates be greater than 1.0 GeV/c to reduce the combinatoric background in identifying X. This ensures that the events are primarily from charm continuum. In order to be consistent with having originated from a D_s^+ decay, the $X\ell^+$ candidates must have an invariant mass less than 1.9 GeV/c^2. For $\eta\ell^+$ candidates, we require that the $\eta\ell^+$ invariant mass be greater than 1.2 GeV/c^2 since backgrounds are large below 1.2 GeV/c^2. In addition, we require that the $X\ell^+$ momentum be between 2.5 and 4.5 GeV/c to reduce random $X\ell^+$ combinations. Since the lepton and X are associated with the same jet, we require that they be in the same hemisphere with respect to the thrust axis.

The Monte Carlo $D_s^+ \to X\ell^+\nu$ events are generated with an event generator which uses the predictions of the ISGW model [4] as input. These events are then passed through a full simulation of the CLEO II detector and the same event reconstruction and analysis chain as the data.

Figure 1(a) shows the K^+K^- invariant mass distribution for all $\phi\ell^+$ combinations which pass the above selection criteria. We fit the distribution with a signal and a background function. The signal function is a Gaussian function convoluted with a Breit-Wigner function. The background function is a phase-space background function [16] which accounts for random K^+K^- combinations. The width of the Breit-Wigner function is fixed to the natural width of the ϕ state [3], and the mean and sigma of the Gaussian function are fixed to the values extracted from a fit to inclusive ϕ candidates with momenta above 1.0 GeV/c. Only the overall normalization of the signal function is allowed to vary in the fits. The number of events found in this and the other channels are given in Table I.

Figure 1(b) shows the $\gamma\gamma$ invariant mass distribution for all $\eta\ell^+$ combinations which pass the above selection criteria. We fit the distribution with a signal and a background function. The signal function is an asymmetric Gaussian function with different sigmas for either side of the mean to account for the detector response to photons. The background function is an exponential function which accounts for random $\gamma\gamma$ combinations. The mean and sigmas of the asymmetric Gaussian function are fixed to the values extracted from a fit to inclusive η candidates with momenta above 1.0 GeV/c.

Figure 1(c) shows the $\eta\pi^+\pi^-$ invariant mass distribution of all $\eta'\ell^+$ combinations which pass the above selection criteria. We fit the distribution with a signal and a background function. The signal function is a Gaussian function. The background function is a first order Chebyshev polynomial function which accounts for random $\eta\pi^+\pi^-$ combinations. The mean and sigma of the Gaussian function are fixed to the values extracted from a fit to inclusive η' candidates with momenta above 1.0 GeV/c.

There are two main sources of background in the sample: X's accompanied by fake leptons [17], and random $X\ell^+$ combinations. The background due to fake leptons is estimated by first using the real data to measure the momentum dependent probabilities that a hadron will be misidentified as a lepton. These probabilities are typically 0.3% for electrons and 1.2% for muons. To estimate the number of events due to fake leptons we take the events which pass the basic event selection cuts. We treat all charged tracks in these events which do not pass the lepton identification criteria as leptons. The entries which pass all the cuts are multiplied by the appropriate fake probability and summed to give the fake background.

For the range of lepton momenta considered, random $X\ell^+$ combinations come from two sources: from $e^+e^- \to c\bar{c}$ events in which an X produced in the fragmentation process is combined with a lepton from a semileptonic decay of the charmed hadron in the same jet, and from $\Upsilon(4S) \to B\bar{B}$ events in which an X produced in the decay chain of one of the B mesons is combined with a lepton from a semileptonic decay of the other B meson. The background from random $X\ell^+$ combinations is estimated using the Monte Carlo simulation. However, the X production rate from both fragmentation and B meson decays is not well known. For this reason, the Monte Carlo prediction is scaled to account for the X production rate observed in the data.

In the charm continuum events, leptons come primarily from the charm semileptonic decays. Therefore the direction of a charmed hadron is close to that of the high momentum lepton. In these events, not only the rate of X production, but also the correlation between the X and the charmed hadron direction is important. The agreement between the data and the Monte Carlo simulation is investigated by considering how often an X is produced in the same hemisphere as a fully reconstructed D meson. The D^0 and D^{*+} mesons are reconstructed using the following decay chains: $D^{*+} \to D^0\pi^+$ and $D^0 \to K^-\pi^+$. The reconstructed D mesons are required to have momenta above 2.5 GeV/c in order to account for the range of D momenta which are expected to contribute leptons in the momentum range of interest. For this particular study, the X momentum criterion is relaxed to 0.8 GeV/c in order to provide sufficient statistics. In doing this we have assumed that the X momentum distribution is well reproduced by the Monte Carlo simulation, and that it is the rate of X production in the fragmentation process which contributes the greatest uncertainty. The yields of D and X mesons produced in the same hemisphere are obtained by fitting their invariant mass distributions. D meson combinatoric backgrounds are accounted for by subtracting the number of X's found in the D meson invariant mass sidebands.

In data 1.2 ± 0.5 η mesons are found for every 1000 reconstructed D mesons. This is to be compared with 1.7 ± 0.1 η mesons per 1000 D mesons in the $e^+e^- \to c\bar{c}$ Monte Carlo sample. Therefore for $D_s^+ \to \eta\ell^+\nu$ we need to scale the Monte Calro estimate of the charm continuum background by the factor of 0.7 ± 0.3. The scale factors for $D_s^+ \to \phi\ell^+\nu$ and $D_s^+ \to \eta'\ell^+\nu$ are 1.0 ± 0.7 and $0.0^{+0.4}_{-0.0}$, respectively. With these factors applied, the Monte Carlo simulation predicts $23.1 \pm 0.8 \pm 15.7$ charm continuum background events for $D_s^+ \to \phi\ell^+\nu$, $35.1 \pm 2.0 \pm 14.1$ for $D_s^+ \to \eta\ell^+\nu$ and $0.0 \pm 0.0^{+3.9}_{-0.0}$ for $D_s^+ \to \eta'\ell^+\nu$ where the first errors are statistical and the second errors are systematic.

The background from random $X\ell^+$ combinations in $B\bar{B}$ events is estimated in a similar manner. In this case the directions of the X and lepton are uncorrelated. For this reason it is sufficient to compare the number of X's with momentum above 1.0 GeV/c in the continuum subtracted $\Upsilon(4S)$ data with the number observed in the $\Upsilon(4S)$ $B\bar{B}$ Monte Carlo sample. In data 7.4 ± 0.8 η mesons are found for every 1000 $B\bar{B}$ events, which is to be compared with 6.4 ± 0.1 in the $B\bar{B}$ Monte Carlo sample. Therefore we need to scale the Monte Calro estimate of the $B\bar{B}$ background for $D_s^+ \to \eta\ell^+\nu$ by the factor of 1.1 ± 0.1. The scale factors for $D_s^+ \to \phi\ell^+\nu$ and $D_s^+ \to \eta'\ell^+\nu$ are 1.0 ± 0.1 and 0.3 ± 0.2, respectively. After these factors are applied, the predicted backgrounds from $B\bar{B}$ events are $49.6 \pm 1.8 \pm 4.1$ events for $D_s^+ \to \phi\ell^+\nu$ $27.6 \pm 2.5 \pm 3.1$ for $D_s^+ \to \eta\ell^+\nu$ and $1.9 \pm 0.2 \pm 1.5$ for $D_s^+ \to \eta'\ell^+\nu$.

For $D_s^+ \to \eta\ell^+\nu$ decay, we have estimated the possible contamination from the decays $D_s^+ \to \eta'\ell^+\nu$ using the Monte Carlo simulation. Due to the hard momentum cuts on the η and $\eta\ell^+$, the efficiency is found to be small, 0.27%, which is about 1/8 of that for $D_s^+ \to \eta\ell^+\nu$ decay. We have an efficiency corrected yield of 7128 ± 1786 events for the $D_s^+ \to \eta'\ell^+\nu$ decay in our data sample, as discussed below. Considering the branching fractions for $\eta' \to \eta\pi^+\pi^-$, $\eta' \to \eta\pi^0\pi^0$ and $\eta \to \gamma\gamma$, we estimate $5.0 \pm 1.3 \pm 1.0$ events from the $D_s^+ \to \eta'\ell^+\nu$ feed down.

We estimate the possible contamination from the Cabibbo suppressed $D^+ \to \eta\ell^+\nu$ decay, which is relatively large since we do not distinguish D_s^+ from D^+. We estimate the ratio of the number of $D^+ \to \eta\ell^+\nu$ events to the number of $D_s^+ \to \eta\ell^+\nu$ events, $R_c^\eta \equiv N(D^+ \to \eta\ell^+\nu)/N(D_s^+ \to \eta\ell^+\nu) = 0.17$ [19]. We calculate the final signal yield for $D_s^+ \to \eta\ell^+\nu$ decay as $N_{signal} = (N_{candidates} - N_{fake\ lepton} - N_{c\bar{c}} - N_{B\bar{B}} - N_{D_s^+ \to \eta'\ell^+\nu\ feed\ down}) \times f_c^\eta$ where $f_c^\eta \equiv 1/(1 + R_c^\eta)$, and obtain 325.6 ± 26.1 events.

In the same manner we estimate the ratio of the number of $D^+ \to \eta'\ell^+\nu$ events to that of $D_s^+ \to \eta'\ell^+\nu$ events, $R_c^{\eta'} \equiv N(D^+ \to \eta'\ell^+\nu)/N(D_s^+ \to \eta'\ell^+\nu) = 0.08$ [19]. We calculate the final signal yield for $D_s^+ \to \eta'\ell^+\nu$ decay as $N_{signal} = (N_{candidates} - N_{fake\ lepton} - N_{c\bar{c}} - N_{B\bar{B}}) \times f_c^{\eta'}$ where $f_c^{\eta'} \equiv 1/(1 + R_c^{\eta'})$, obtain 29.1 ± 7.3 events.

Figure 2(a), Figure 2(b) and Figure 2(c) show the number of ϕ's, η's and η''s which fall in each bin of the $\phi\ell^+$, $\eta\ell^+$ and $\eta'\ell^+$ mass, respectively. The combined background estimate is also shown, as well as the sum of the simulated signal shape and the combined background estimate. The simulated signal shape has been normalized to the number of candidates extracted from the fit to the K^+K^-, $\gamma\gamma$ and $\pi^+\pi^-\gamma\gamma$ invariant mass spectra. Table I gives the yields after correcting for efficiencies and the $\phi \to K^+K^-$, $\eta \to \gamma\gamma$ and $\eta' \to \eta\pi^+\pi^-$ branching fractions [3].

TABLE I. Summary of $D_s^+ \to \phi\ell^+\nu$, $D_s^+ \to \eta\ell^+\nu$ and $D_s^+ \to \eta'\ell^+\nu$ yields for the non D_s^{*+} tag analysis. The errors quoted in this table are statistical only.

Decay mode	$D_s^+ \to \phi\ell^+\nu$	$D_s^+ \to \eta\ell^+\nu$	$D_s^+ \to \eta'\ell^+\nu$
Candidates	863.6 ± 40.5	577.6 ± 30.3	42.3 ± 7.9
Fake lepton background	95.3 ± 2.2	128.8 ± 1.6	9.0 ± 0.4
Continuum $c\bar{c}$ background	23.1 ± 0.8	35.1 ± 2.0	0.0 ± 0.0
$B\bar{B}$ background	49.6 ± 1.8	27.6 ± 2.5	1.9 ± 0.2
$D_s^+ \to \eta'\ell^+\nu$ feed down		5.0 ± 1.3	
$D_s^+ + D^+$	695.6 ± 40.6	381.0 ± 30.5	31.4 ± 7.9
f_c		0.855	0.926
D_s^+ signal yield	695.6 ± 40.6	325.6 ± 26.1	29.1 ± 7.3
Efficiency, $\epsilon \cdot \mathcal{B}$ (%)	2.078	0.807	0.204
Efficiency corrected yield	16734 ± 976	20184 ± 1616	7128 ± 1786

To get the effective yield in the electron channel, we need to take into account the reduction of the muon rate relative to the electron rate due to the reduced phase space [13], and the efficiency loss in the electron rate due to the final state radiation [18], which are not simulated in the Monte Carlo. With these corrections applied, the ratios of branching fractions measured with the non D_s^{*+} tag method are

$$R_{\eta/\phi} = \frac{\mathcal{B}(D_s^+ \to \eta e^+\nu)}{\mathcal{B}(D_s^+ \to \phi e^+\nu)} = 1.21 \pm 0.12 \pm 0.16, \tag{1}$$

$$R_{\eta'/\phi} = \frac{\mathcal{B}(D_s^+ \to \eta' e^+\nu)}{\mathcal{B}(D_s^+ \to \phi e^+\nu)} = 0.43 \pm 0.11 \pm 0.07, \tag{2}$$

$$R_{\eta'/\eta} = \frac{\mathcal{B}(D_s^+ \to \eta' e^+\nu)}{\mathcal{B}(D_s^+ \to \eta e^+\nu)} = 0.35 \pm 0.09 \pm 0.07, \tag{3}$$

where the first error is statistical, and the second is systematic in each ratio. Table II summarizes the systematic errors in the non D_s^{*+} tag analysis.

TABLE II. The break down of systematic errors (%) in the non D_s^{*+} tag analysis

Decay mode	$D_s^+ \to \phi e^+ \nu$	$D_s^+ \to \eta e^+ \nu$	$D_s^+ \to \eta' e^+ \nu$
$c\bar{c}$ BG	2.3	3.7	12.5
$B\bar{B}$ BG	0.6	0.8	4.7
K/π particle ID	3.0		3.0
η reconstruction		5.0	5.0
$D_s^+ \to \eta' \ell^+ \nu$ feed down		0.3	
f_c		6.0	2.8
Fit	3.0	5.0	3.0
MC stat	1.2	1.5	2.5
Fragmentation	1.1	1.1	1.1
ϕ polarization	1.0		
Lepton fake rate	4.1	10.1	8.6
Tracking	6.0	2.0	6.0

In the D_s^{*+} tag analysis, we look for a low energy photon from the $D_s^{*+} \to D_s^+ \gamma$ decay along with an energetic pair of a lepton and an $X(\equiv \phi$ or $\eta)$ in the same jet. To obtain more statistics we lower the electron momentum cut to 0.7 GeV/c and the $X\ell^+$ momentum cut to 2.0 GeV/c. The rest of the cuts for selecting leptons, X's and $X\ell^+$'s are the same as for the non D_s^{*+} tag analysis.

After selecting $X\ell^+$ candidates which pass the above criteria, we then combine them with a photon which lies in the same hemisphere with respect to the thrust axis. The photon must lie in the fiducial region, $|\cos\theta| < 0.71$, and have energy greater than 0.12 GeV. We require that the lateral shower shape of the photon be consistent with that expected for a true photon. To further suppress background photons from π^0 decays, we veto all $\gamma\gamma$ combinations that fall within 2.5σ of the π^0 mass. To select $X\ell^+\gamma$ candidates which come from the $D_s^{*+} \to D_s^+\gamma$, we require that $\Delta M \equiv M_{X\ell^+\gamma} - M_{X\ell^+}$ be between 0.1 and 0.2 GeV/c^2, where $M_{X\ell^+}$ and $M_{X\ell^+\gamma}$ are the invariant masses of $X\ell^+$ and $X\ell^+\gamma$ systems, respectively.

Figure 3(a) and (b) show the K^+K^- and $\gamma\gamma$ invariant mass distributions for all $\phi\ell^+\gamma$ and $\eta\ell^+\gamma$ combinations which pass the above selection criteria. The number of events found in these channels are given in Table III.

The backgrounds due to fake leptons, random $X\ell^+$ combinations the $D_s^+ \to \eta'\ell^+\nu$ feed down are estimated by the same procedure as for the non D_s^{*+} tag analysis. Also with a Monte Carlo simulation, we estimate the possible contamination from the Cabibbo suppressed decay mode $D^+ \to \eta\ell^+\nu$ to the $D_s^+ \to \eta\ell^+\nu$ decay, which turns out to be small because of the requirement of the photon from the D_s^{*+}. These backgrounds are listed in Table III.

The background from the combinations of a true $X\ell^+$ and a random photon is estimated using a Monte Carlo simulation. To test the agreement between the Monte Carlo estimate and the data for this background, we use the events with the decay chain, $D^{*+} \to D^0\pi^+$ and $D^0 \to K^-e^+\nu$. These events are ideally suited for the test because the K^-e^+ pair has a similar kinematics as the $X\ell^+$ pair from D_s^+, and any photons associated with a K^-e^+ pair in the same jet are ensured to be not from D_s^{*+}. We investigate how often a K^-e^+ pair from this decay chain combined with a random photon falls in the ΔM region of interest. First we find K^-e^+ pairs with the same $X\ell^+$ selection criteria as discussed before, and fit the $M_{K^-e^+\pi^+} - M_{K^-e^+}$ distribution to reconstruct the decay chain $D^{*+} \to D^0\pi^+$ and $D^0 \to K^-e^+\nu$. The fit gives 3038 ± 56 K^-e^+ pairs in the Monte Carlo sample and 1059 ± 34 in the data sample. Then we combine random photons with the K^-e^+ pairs and calculate ΔM as described for $D_s^+ \to X\ell^+\nu$. Finally we refit the $M_{K^-e^+\pi^+} - M_{K^-e^+}$ distribution for the $K^-e^+\gamma$ combinations falling in $0.1 < \Delta M < 0.2$ GeV/c^2. The refit gives 676 ± 26 K^-e^+ pairs for the Monte Carlo sample and 226 ± 16 for the data sample. The random photon background probability is $(22.3 \pm 0.1)\%$ for the Monte Carlo and $(21.4 \pm 1.7)\%$ for the data. Therefore we need to scale the Monte Carlo estimate of the random photon background by the factor of 0.96 ± 0.08. With this scaling factor, the Monte Carlo simulation predicts the ratio of the signal to the sum of the signal and the random photon background, f_{sig}, to be 0.759 for $D_s^+ \to \phi\ell^+\nu$ and 0.803 for $D_s^+ \to \eta\ell^+\nu$ after all other backgrounds have been subtracted. The results are given in in Table III.

Figure 3(c) and Figure 3(d) show the number of ϕ's and η's which fall in each ΔM bin, respectively. The combined background estimate is also shown, as well as the sum of the simulated signal shape and the combined background estimate. The simulated signal shape has been normalized to the number of candidates extracted from the fit to the K^+K^- and $\gamma\gamma$ invariant mass spectra.

TABLE III. Summary of $D_s^+ \to \eta\ell^+\nu$ and $D_s^+ \to \phi\ell^+\nu$ yields for the D_s^{*+} tag analysis. The errors quoted in this table are statistical only.

Decay mode	$D_s^+ \to \phi\ell^+\nu$	$D_s^+ \to \eta\ell^+\nu$
Candidates	326.9 ± 27.1	153.4 ± 15.0
Fake lepton background	27.9 ± 1.2	22.7 ± 0.7
Continuum $c\bar{c}$ background	15.6 ± 0.7	8.5 ± 1.0
$B\bar{B}$ background	7.9 ± 0.7	3.8 ± 1.0
$D_s^+ \to \eta'\ell^+\nu$ feed down		2.3 ± 0.6
$D^+ \to \eta\ell^+\nu$ contamination		1.3 ± 0.1
D_s^{*+} + Random photon background	275.5 ± 27.2	114.8 ± 15.1
f_{sig}	0.759	0.803
D_s^{*+} signal yield	209.2 ± 20.6	92.2 ± 12.1
Efficiency, $\epsilon \cdot \mathcal{B}$ (%)	1.408	0.474
Efficiency corrected yield	7431 ± 733	9730 ± 1276

Again we need to take into account the reduction of the muon rate relative to the electron rate due to the reduced phases pace [13] and the efficiency loss in the electron rate due to final state radiation [18] to get the effective yield in the electron channel. With these corrections applied, the ratio of branching fractions measured with the D_s^{*+} tag method is,

$$R_{\eta/\phi} = \frac{\mathcal{B}(D_s^+ \to \eta e^+\nu)}{\mathcal{B}(D_s^+ \to \phi e^+\nu)} = 1.32 \pm 0.22 \pm 0.15. \quad (4)$$

Table IV summarizes systematic errors in the D_s^{*+} tag analysis.

TABLE IV. The break down of systematic errors (%) in the D_s^{*+} tag analysis

Decay mode	$D_s^+ \to \phi e^+ \nu$	$D_s^+ \to \eta e^+ \nu$
$c\bar{c}$ BG	3.8	3.0
$B\bar{B}$ BG	0.2	0.3
K particle ID	3.0	
η reconstruction		5.0
$D_s^+ \to \eta' \ell^+ \nu$ feed down		0.4
$D^+ \to \eta \ell^+ \nu$ contamination		0.3
Fit	3.0	5.0
MC stat	1.7	2.1
Fragmentation	1.1	1.1
ϕ polarization	1.0	
Lepton fake rate	3.0	5.9
f_{sig}	2.9	2.2
Tracking	6.0	2.0

We combine the measurements for $\mathcal{B}(D_s^+ \to \eta e^+ \nu)/\mathcal{B}(D_s^+ \to \phi e^+ \nu)$ from the non D_s^{*+} tag and the D_s^{*+} tag methods. We find that only 21% of the non tag sample overlaps with the tag sample. Considering this overlapping fraction, the two measurements are consistent. The non tag measurement is statistically more significant than the tag measurement, but it has a large systematic uncertainty due to the $D^+ \to \eta \ell^+ \nu$ contamination.

We separate the sytematic errors into correlated and uncorrelated contributions in the two measurements. We form the weight for each measurement using the statistical and uncorrelated systematic errors, and determine the combined result from the weighted average of the two measurements. We find the weighted average of the two $\mathcal{B}(D_s^+ \to \eta e^+ \nu)/\mathcal{B}(D_s^+ \to \phi e^+ \nu)$ measurements to be :

$$R_{\eta/\phi} = \frac{\mathcal{B}(D_s^+ \to \eta e^+ \nu)}{\mathcal{B}(D_s^+ \to \phi e^+ \nu)} = 1.24 \pm 0.12 \pm 0.15. \tag{5}$$

Model predictions and measurements are listed in Table V including our new measurements. Our measurements of $R_{\eta/\phi}$ and $R_{\eta'/\phi}$ agree well with the ISGW2 model predictions with an $\eta - \eta'$ mixing angle of -10° [11]. The predictions of Kamal *et al.* for $R_{\eta/\phi}$ and $R_{\eta'/\phi}$ are higher than our measurements [22–24]. E653 reported an upper limit on $R_{\eta'/\phi}$ and a measurement of $R_{\eta/\phi} + R_{\eta'/\phi} = 3.9 \pm 1.6$ using the muon channel [12].

Table VI lists the measurements and predictions of the ratio of vector to pseudoscalar rates for D_s^+ and D semileptonic decays [1–3]. Our measurement of the vector to pseudoscalar ratio for the D_s^+ semileptonic decay, *i.e.*, $\mathcal{B}(D_s^+ \to \phi e^+ \nu)/\mathcal{B}(D_s^+ \to (\eta + \eta')e^+ \nu) = 1/(R_{\eta/\phi} + R_{\eta'/\phi}) = 0.60 \pm 0.06 \pm 0.06$, agrees well with the measurement for D semileptonic decays, and also with the ISGW2 model prediction [11].

The factorization hypothesis, which relates the semileptonic process $D_s^+ \to (\eta, \eta')e^+ \nu$ directly to the hadronic process $D_s^+ \to (\eta, \eta')\rho^+$, predicts $\mathcal{B}(D_s^+ \to \eta' e^+ \nu)/\mathcal{B}(D_s^+ \to \eta e^+ \nu) =$

TABLE V. Summary of predictions and measurements. ISGW2 predicts $R_{\eta/\phi}$ and $R_{\eta'/\phi}$ for the $\eta-\eta'$ mixing angle of $-10°$ and $-20°$. The numbers in the parentheses are for $-20°$.

Predictions and Measurements	$R_{\eta/\phi}$	$R_{\eta'/\phi}$	$R_{\eta/\phi}+R_{\eta'/\phi}$
ISGW2 [11]	1.17 (0.77)	0.50 (0.67)	1.67 (1.44)
Kamal *et al.* [22–24]	1.85 ± 0.56	2.22 ± 0.72	4.07 ± 0.91
E653 [12]		< 1.6 @90%C.L.	3.9 ± 1.6
This result	$1.24 \pm 0.12 \pm 0.15$	$0.43 \pm 0.11 \pm 0.07$	$1.67 \pm 0.16 \pm 0.17$

TABLE VI. Summary of the ratio of vector to pseudosclar rates for D_s^+ and D semileptonic decays. ISGW2 predicts the ratio in D_s^+ sector for the $\eta-\eta'$ mixing angle of $-10°$ and $-20°$. The number in the parenthesis is for $-20°$.

	This result	ISGW2 [11]
$\mathcal{B}(D_s^+ \to \phi e^+\nu)/\mathcal{B}(D_s^+ \to (\eta+\eta')e^+\nu)$	$0.60 \pm 0.06 \pm 0.06$	0.60 (0.69)
	World Average [1–3]	ISGW2 [11]
$\mathcal{B}(D \to \overline{K^*}e^+\nu)/\mathcal{B}(D \to \overline{K}e^+\nu)$	0.56 ± 0.06	0.54

$\mathcal{B}(D_s^+ \to \eta'\rho^+)/\mathcal{B}(D_s^+ \to \eta\rho^+)$ [22]. We obtain $\mathcal{B}(D_s^+ \to \eta'\rho^+)/\mathcal{B}(D_s^+ \to \eta\rho^+) = 1.20 \pm 0.35$ by combining CLEO II measurements of $\mathcal{B}(D_s^+ \to \eta\rho^+)/\mathcal{B}(D_s^+ \to \phi\pi^+)$ and $\mathcal{B}(D_s^+ \to \eta'\rho^+)/\mathcal{B}(D_s^+ \to \phi\pi^+)$ [23]. It disagrees with our measurement of $\mathcal{B}(D_s^+ \to \eta' e^+\nu)/\mathcal{B}(D_s^+ \to \eta e^+\nu) = 0.35 \pm 0.09 \pm 0.07$.

In conclusion, we have measured $\mathcal{B}(D_s^+ \to \eta e^+\nu)/\mathcal{B}(D_s^+ \to \phi e^+\nu) = 1.24 \pm 0.12 \pm 0.15$ and $\mathcal{B}(D_s^+ \to \eta' e^+\nu)/\mathcal{B}(D_s^+ \to \phi e^+\nu) = 0.43 \pm 0.11 \pm 0.07$. These are the first measurements of these quantities. Our value for the ratio of vector to pseudoscalar rates for the D_s^+ semileptonic decays agrees with that observed for the D^+ and D^0 semileptonic decays, and also with the ISGW2 model prediction. This agreement enhances confidence in the evaluations of the $D_s^+ \to \phi\pi^+$ branching ratio using models of semileptonic decays and measurements of $\Gamma(D_s^+ \to \phi\ell^+\nu)/\Gamma(D_s^+ \to \phi\pi^+)$ [25].

ACKNOWLEDGEMENTS

We gratefully acknowledge the effort of the CESR staff in providing us with excellent luminosity and running conditions. This work was supported by the National Science Foundation, the U.S. Department of Energy, the Heisenberg Foundation, the Alexander von Humboldt Stiftung, the Natural Sciences and Engineering Research Council of Canada, and the A.P. Sloan Foundation.

REFERENCES

[1] Note that we do not distinguish D^+ and D^0 for the ratio of vector to pseudoscalar rates for D mesons.

[2] For all states described, the charge conjugate state is also implied.

[3] Particle Data Group, L. Montanet *et al.*, Review of Particle Properties, Phys. Rev. D **50** (1994) 1173.

[4] N. Isgur *et al.*, Phys. Rev. D **39** (1989) 799.

[5] M. Wirbel *et al.*, Z. Phys. C **39** (1985) 627; and J.G. Körner and G.A. Schuler, Z. Phys. C **38** (1988) 511.

[6] T. Altomari and L. Wolfenstein, Phys. Rev. D **37** (1988) 681; and F.J. Gilman and R.L. Singleton, Phys. Rev. D **41** (1990) 142.

[7] V. Lubicz *et al.*, Phys. Lett. B **274** (1992) 415.

[8] C. Bernard *et al.*, Phys. Rev. D **43** (1991) 2140 and Phys. Rev. D **47** (1993) 998.

[9] A. Abada *et al.*, ELC and APE Collaborations, in Lattice '93, Nucl. Phys. B (Proc. Suppl.) **34** (1994) 477; APE: C.R. Allton *et al.*, ROME prep. 94/1050.

[10] P. Ball *et al.*, Phys. Lett. B **259** (1991) 481; P. Ball *et al.*, Phys. Rev. D **44** (1991) 3567

[11] D. Scora and N. Isgur, preprint CEBAF-TH-94-14.

[12] E653 Collaboration, K. Kodama *et al.*, Phys. Lett. B **309** (1993) 483.

[13] J.G. Körner and G.A. Schuler, Z. Phys. C **46** (1990) 93. The rates of $D_s^+ \to \phi\mu^+\nu$, $D_s^+ \to \eta\mu^+\nu$ and $D_s^+ \to \eta'\mu^+\nu$ are 5%, 3% and 5%, respectively, lower than those of electron channels due to the reduced phase space.

[14] CLEO Collaboration, Y. Kubota *et al.*, Nucl. Inst. and Meth. **A320** (1992) 66.

[15] G.C. Fox and S. Wolfram, Phys. Rev. Lett. **41** (1978) 1581.

[16] The phase space background function has the form: $a \cdot (m - m_0)^\alpha \cdot e^{-\beta(m-m_0)}$, where m is the invariant mass of the K^+K^- pair. The parameter m_0 is obtained from a fit to the inclusive K^+K^- invariant mass distribution and is fixed in fitting the $D_s^+ \to \phi\ell^+\nu$ signal; α and β are free parameters.

[17] Fake leptons are either misidentified hadrons or muons from π^+ and K^+ decays in flight.

[18] D. Atwood and W.J. Marciano, Phys. Rev. D **41** (1990) 1736. Final state radiation reduces the detection efficiencies of $D_s^+ \to \phi e^+\nu$, $D_s^+ \to \eta e^+\nu$ and $D_s^+ \to \eta' e^+\nu$ by 1.1%, 2.5% and 1.1% respectively, and has a negligible effect in the muon channels.

[19] The ratio of the number of $D^+ \to \eta(\eta')\ell^+\nu$ events to the number of $D_s^+ \to \eta(\eta')\ell^+\nu$ events can be written as:

$$R_c^\eta(R_c^{\eta'}) \equiv \frac{N(D^+ \to \eta(\eta')\ell^+\nu)}{N(D_s^+ \to \eta(\eta')\ell^+\nu)} = \frac{\sigma(D^+)}{\sigma(D_s^+)} \cdot \frac{\Gamma(D^+ \to \eta(\eta')\ell^+\nu)}{\Gamma(D_s^+ \to \eta(\eta')\ell^+\nu)} \cdot \frac{\tau_{D^+}}{\tau_{D_s^+}}.$$

CLEO 1.5 measured $\sigma(D^+) \cdot \mathcal{B}(D^+ \to K^-\pi^+\pi^+)/\sigma(D_s^+) \cdot \mathcal{B}(D_s^+ \to \phi\pi^+) = (48.8 \pm 4.8)/(7.4 \pm 1.2) = 6.6 \pm 1.3$ [20]. Using CLEO II measurement of $\mathcal{B}(D^+ \to K^-\pi^+\pi^+) = (9.3 \pm 1.0)\%$ [21] and the world average for $\mathcal{B}(D_s^+ \to \phi\pi^+)$ [3], we obtain $\sigma(D^+)/\sigma(D_s^+) = 2.5 \pm 0.8$. ISGW2 predicts $\Gamma(D^+ \to \eta(\eta')\ell^+\nu)/\Gamma(D_s^+ \to \eta(\eta')\ell^+\nu)$ in units of $|V_{cd}|^2/|V_{cs}|^2$ to be 0.39 (0.38) for $\theta_m = -10^\circ$, and 0.81 (0.19) for $\theta_m = -20^\circ$ where θ_m is the η-η' mixing angle [11]. We use $|V_{cd}|^2/|V_{cs}|^2 = 0.051$ and the world averages for the lifetime of D^+ and D_s^+ [3]. We find $R_c^\eta(R_c^{\eta'})$ to be 0.11 ± 0.03 (0.11 ± 0.03) for $\theta_m = -10^\circ$ and 0.23 ± 0.06 (0.06 ± 0.01) for $\theta_m = -20^\circ$. For θ_m ranging between -10° and -20°, we estimate $R_c^\eta(R_c^{\eta'}) = 0.17 \pm 0.07$ (0.08 ± 0.03)

[20] CLEO Collaboration, R. Ammar *et al.*, Phys. Rev. D **44** (1991) 3583.
[21] CLEO Collaboration, R. Balest *et al.*, Phys. Rev. Lett. **72** (1993) 2328.
[22] A.N. Kamal *et al.*, Phys. Rev. D **49** (1994) 1330. Combining the factorization hypothesis with the measurements of $\mathcal{B}(D_s^+ \to \eta\rho^+)/\mathcal{B}(D_s^+ \to \phi\pi^+)$ and $\mathcal{B}(D_s^+ \to \eta'\rho^+)/\mathcal{B}(D_s^+ \to \phi\pi^+)$ [23], Kamal *et al.* predict $\mathcal{B}(D_s^+ \to \eta e^+\nu)/\mathcal{B}(D_s^+ \to \phi\pi^+) = 1.00 \pm 0.19 \pm 0.20$ and $\mathcal{B}(D_s^+ \to \eta' e^+\nu)/\mathcal{B}(D_s^+ \to \phi\pi^+) = 1.20 \pm 0.27 \pm 0.24$. We combine the predictions of Kamal *et al.* and CLEO II measurement for $\mathcal{B}(D_s^+ \to \phi e^+\nu)/\mathcal{B}(D_s^+ \to \phi\pi^+)$ [24] to reach the predictions for $R_{\eta/\phi}$ and $R_{\eta'/\phi}$ quoted in the text.
[23] CLEO Collaboration, P. Avery *et al.*, Phys. Rev. Lett. **68** (1992) 1279.
[24] CLEO Collaboration, F. Butler *et al.*, Phys. Lett. B **324** (1994) 255.
[25] J.D. Richman and P.R. Burchat, preprint UCSB-HEP-95-08 & Stanford-HEP-95-01, to be published in Riviews of Modern Physics. They use the relation

$$\mathcal{B}(D_s^+ \to \phi\pi^+) = F \cdot \mathcal{B}(D^+ \to \overline{K^{*0}}\ell^+\nu) \cdot \frac{\Gamma(D_s^+ \to \phi\pi^+)}{\Gamma(D_s^+ \to \phi\ell^+\nu)} \cdot \frac{\tau_{D_s^+}}{\tau_{D^+}},$$

where F is the theoretical prediction for $\Gamma(D_s^+ \to \phi\ell^+\nu)/\Gamma(D^+ \to \overline{K^{*0}}\ell^+\nu)$. They predict $\mathcal{B}(D_s^+ \to \phi\pi^+) = (3.7 \pm 0.5 \pm 0.4)\%$, where the last uncertainty reflects the range of theoretical predictions for F.

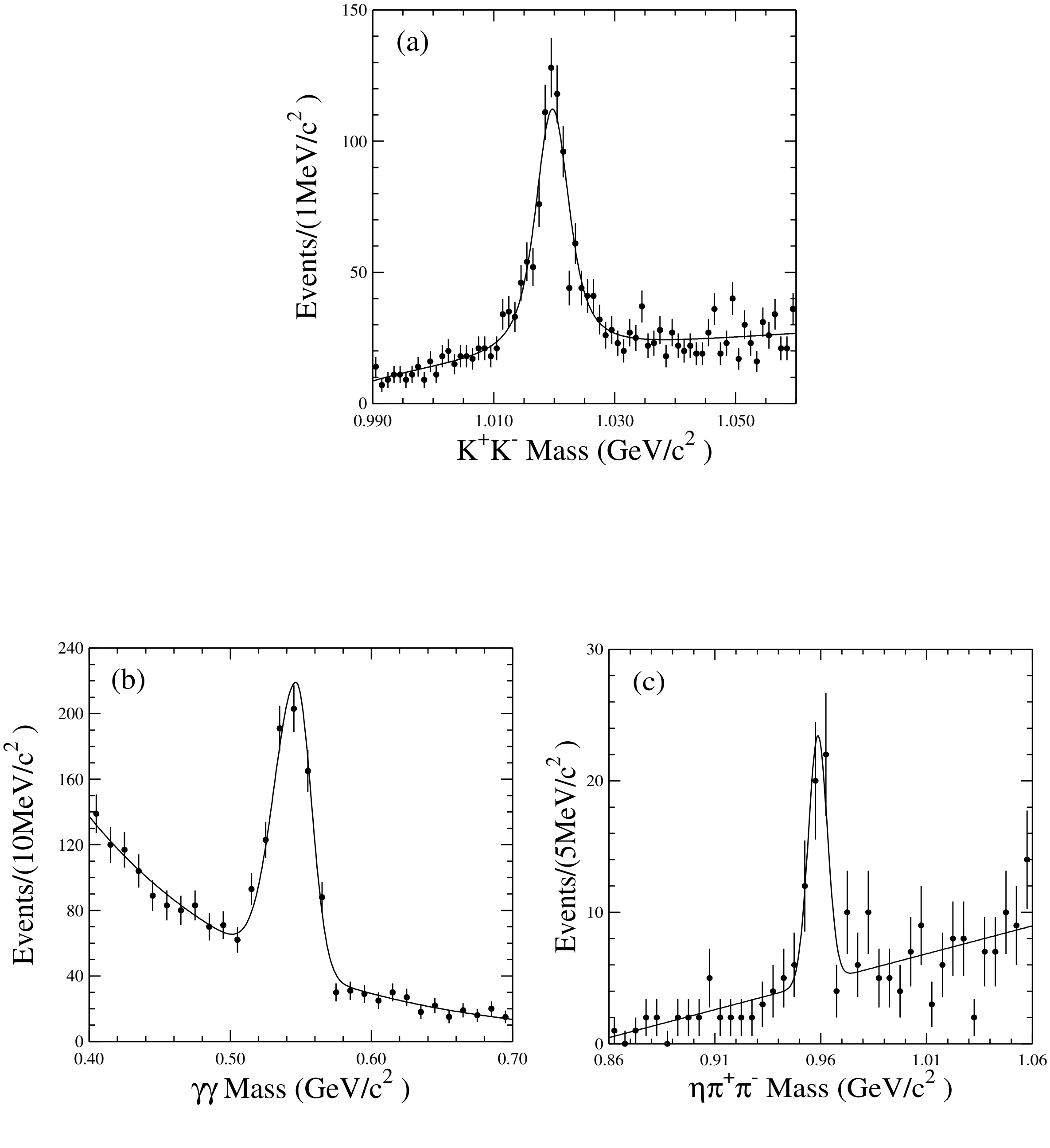

FIG. 1. The K^+K^-, $\gamma\gamma$ and $\eta\pi^+\pi^-$ invariant mass distributions of $D_s^+ \to \phi\ell^+\nu$, $D_s^+ \to \eta\ell^+\nu$ and $D_s^+ \to \eta'\ell^+\nu$ candidates, respectively, for the non D_s^{*+} tag analysis. The curve on each distribution is the fit to the invariant mass distribution.

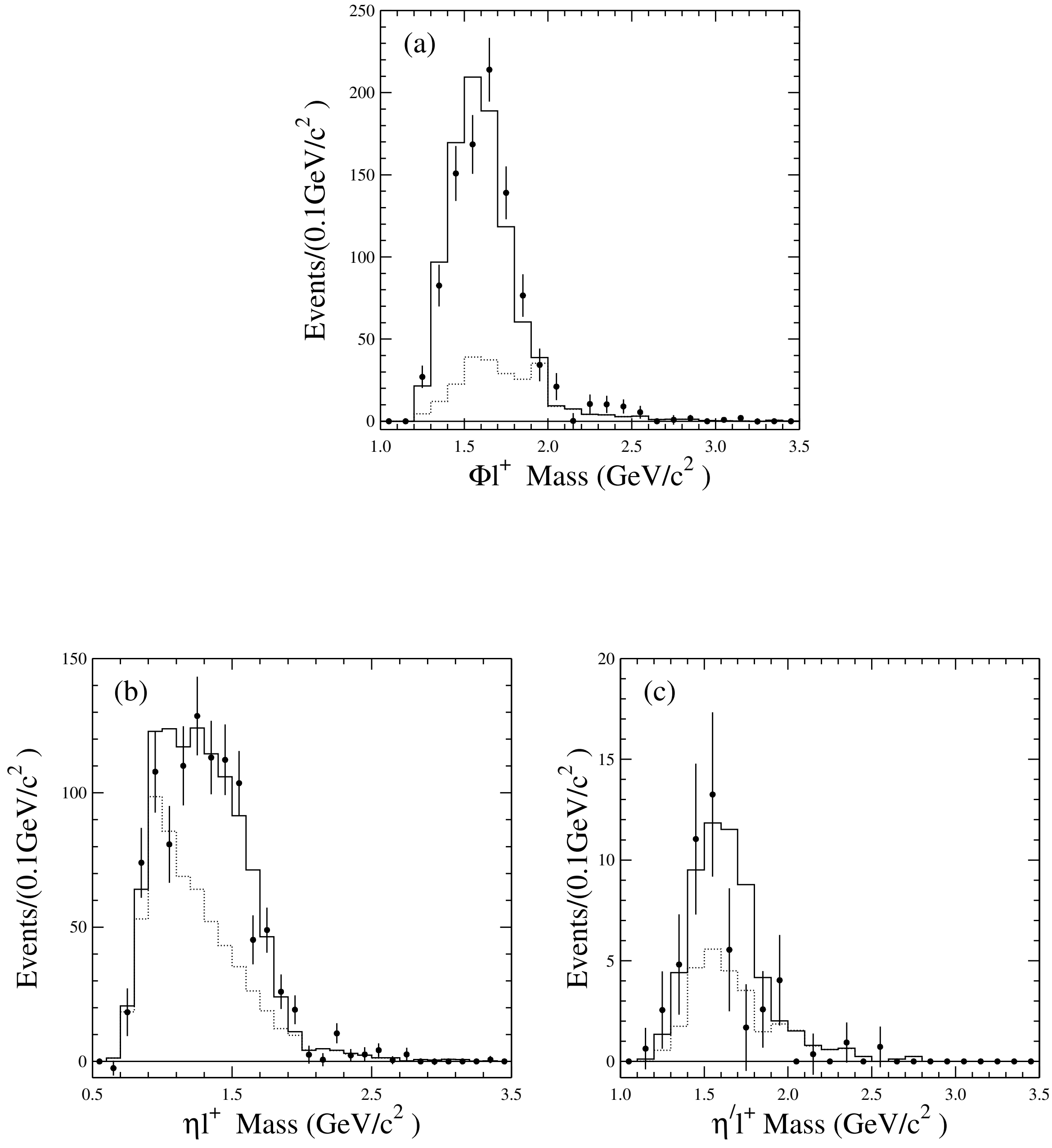

FIG. 2. $M_{X\ell^+}$ distributions of $D_s^+ \to X\ell^+\nu$ ($X \equiv \phi, \eta$ or η') candidates for the non D_s^{*+} tag analysis. The solid circles represent the candidates in each $M_{X\ell^+}$ bin. The solid histogram shows the sum of the simulated signal shape and the predicted background. The dotted histgram shows the predicted background.

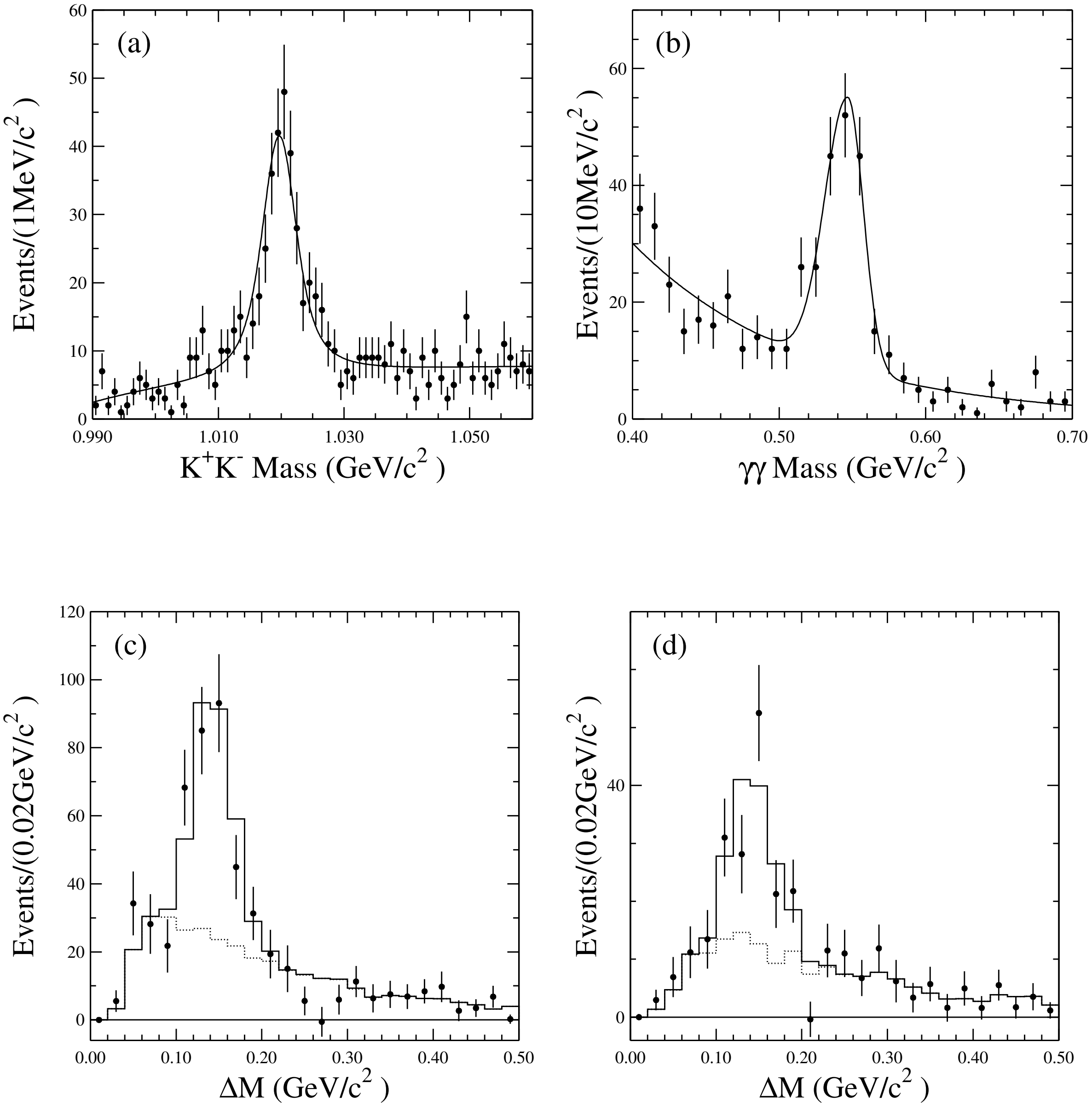

FIG. 3. The top two plots are the K^+K^- and $\gamma\gamma$ invariant mass distributions of $D_s^+ \to \phi\ell^+\nu$ and $D_s^+ \to \eta\ell^+\nu$ candidates for the D_s^{*+} tag analysis. The curve on each distribution is the fit to the invariant mass distribution. The bottom two plots are the distributions of the pseudo mass difference between D_s^{*+} and D_s^+ for $D_s^+ \to \phi\ell^+\nu$ and $D_s^+ \to \eta\ell^+\nu$ candidates. The solid circles represent the candidates in each ΔM bin. The solid histogram shows the sum of the simulated signal shape and the predicted background. The dotted histgram shows the predicted background.